Korean J. Chem. Eng., 39(10), 2834-2841 (2022)
DOI: 10.1007/s11814-022-1218-9

pISSN: 0256-1115
eISSN: 1975-7220

Optical, structural and electrical properties of RuS_2 thin films, obtained at low temperatures by spray pyrolysis

Ghada Bidouk*, Beya Ouertani*,,†, Chaker Bouzidi***, Bertrand Theys****, and Hatem Ezzaouia***

*Research and Technology Center of Energy, Photovoltaic laboratory (LPV),
Borj-Cedria Science and Technology Park, Tunisia
**University of Carthage, Higher Institute of Environmental Science and Technology of Borj Cedria,
Borj-Cedria Science and Technology Park, Tunisia
***Physical Chemistry Laboratory of Mineral Materials and Their Applications,
National Center of Research in Materials Science, Technologic Park of Borj Cedria, Tunisia
****Institut de Recherche et Développement sur l'Energie Photovoltaïque (IRDEP), Unité mixte de recherche
CNRS-EDF-Chimie Paris Tech Institut Photovoltaïque Ile de France (IPVF), 6 Quai Watier, 78401 Chatou, France
(*Received 17 April 2022 • Revised 27 June 2022 • Accepted 29 June 2022*)

Abstract−Aqueous ruthenium (III) chloride ($RuCl_3.3H_2O$) solution (0.03 M) was sprayed on pre-heated ordinary glass substrates. Amorphous ruthenium oxide thin films were obtained, which were sulfurized under vacuum at several lower heat treatment temperatures (400, 450, 500 and 550 °C) in RTP oven. The XRD results indicated the appearance of the RuS_2 phase for all the sulfurization temperatures. The layer compositions were confirmed by EDS analysis. Monocrystalline and polycrystalline RuS_2 thin films were obtained. SEM images showed mix of morphologies (filament, particles, and clusters) with porous surfaces. High absorption coefficients were deduced. The obtained RuS_2-thin films showed different direct band gaps (1.43, 1.80, 1.79, 1.83 eV), which make it a distinct energy conversion and storage material. The opto-electrical properties of the as obtained RuS_2-thin films make them among the best candidats for several applications, such as low cost material for low cost solar cells, and for alkaline hydrogen evolution electrocatalysts.

Keywords: RuS_2, Spray Pyrolysis, Sulfurization, High Absorbance, Monocrystalline and Polycrystalline

INTRODUCTION

Ruthenium sulfides belong to the major group of minerals, which are widely distributed in nature: the family of transition metal sulfides (TMS). Besides, ruthenium sulfide (RuS_2) is a favorable active material. Therefore, RuS_2 has been used in various applications such as photo-electrochemical [1,2], energy conversion [3], thermal catalytic processing [4-7], energy-related technologies, and photocatalytic decomposition of water [8-10]. RuS_2 presents remarkable activity against photo corrosion as well as the ability of absorbing visible light [1]. Then, ruthenium sulfide is the most interesting material among the transition compounds, and it presents the highest catalytic activity for hydrodesulfurization processes (HDS) [11]. This makes it a promising candidate as catalyst and replaces MoS_2 one [4,11-13]. It is also very active for the hydrogenation of the molecules [14]. Ruthenium sulfide is one of several transition metal dichalcogenides that crystallize with a pyrite structure [15-17]. Moreover, it shows good stability against photocorrosion and the evolution of hydrogen and oxygen [18-20]. Higher bias voltage is needed for good photocurrent efficiency [1,19].

Several techniques had been used for growing RuS_2 films. In 1979, Passaretti et al. [21] prepared, successfully, RuS_2 using anhydrous $RuC1_3$ and NH_4HS in 2-methoxyethyl ether at room temperature. Then, in 1990, Le Nagard et al. [22] used bis-cyclopentadienyl ruthenium (ruthenocene) and hydrogen sulfide as precursors for preparing RuS_2 thin films by metalorganic chemical vapor deposition technique (MOCVD). The obtained RuS_2 films, during this work, were grown on various substrates, such as SiO_2, Al_2O_3 and GaAs. In 1994, Ashokkumar et al. [1] coated TiO_2 electrodes with RuS_2 colloids. Thus, the electrodes showed spectral sensitization effect with an increase in the photocurrent response of TiO_2 towards longer wavelength spectral region. In another approach, RuS_2 nanoislands were grown on Au(111) using chemical vapor deposition [14]. Indeed, during this work [14], the RuS_2(111)/Au system provided an excellent model system for ruthenium sulfide catalysts.

Kratzig et al. [19] prepared, for the first time, RuS_2 thin films deposited on (100) and (111)-oriented FeS_2 (pyrite). Using optical reflectance spectroscopy and Seebeck coefficient measurements, a direct band gap of 1.9 eV and p-type conductivity were determined.

Referring to the concentration of several researchers on this material that having interesting properties such as its band gap energy that was reported in different studies to be ~1.8, ~1.9 and ~1.3 eV [1,4,8,15,19,22,23].

Knowing the efficiency, the simplicity, the low cost, the non-toxicity, and the reproducibility of the spray pyrolysis technique for growing thin films [24-29], we thought about its use as a novel method for synthesizing thin films of this interesting material: ruthenium sulfide. Indeed, the obtained RuS_2 layers, using spray pyrolysis tech-

†To whom correspondence should be addressed.
E-mail: Beya.Ouertani@isste.rnu.tn, bouertani@yahoo.fr

nique, may have better optoelectronic properties than those obtained by other techniques. The different optical transitions are deduced by plotting, for each sample, $(\alpha \cdot h \cdot \nu)^2$ vs the photon energy $(h \cdot \nu)$ for the direct ones and $(\alpha \cdot h \cdot \nu)^{1/2}$ vs $(h \cdot \nu)$ for the indirect ones. The band gap is the transition corresponding to the lowest obtained photon energy (direct or indirect), where α is the absorption coefficient.

EXPERIMENTAL DETAILS

Amorphous ruthenium oxide thin films were deposited on ordinary glass substrates by spray pyrolysis. Then, the obtained films were heat treated under sulfur atmosphere. In a first step, the glass substrates were cleaned in aqua regia (mixture of concentrated nitric and hydrochloric acids), then in acetone, and finally in deionized water during 15 min for each step. After their cleaning, they were put in an oven for drying. In a second step, ruthenium (III) chloride ($RuCl_3 \cdot 3H_2O$) aqueous solution (0.03 M) was prepared.

The ionization reaction of water is written according to the following equation:

$$2H_2O \rightarrow H_3O^+ + OH^- \quad (1)$$

And after dissolving the $RuCl_3 \cdot 3H_2O$ (black powder) in deionized water, its ionization reaction is according to the following equation [30]:

$$2Ru\ (III)Cl_3 \rightarrow 2Ru^{3+} + 6Cl^- \quad (2)$$

The cations (Ru^{3+}) get complexed with (OH^-) forming ruthenium hydroxide, according to the following reaction:

$$Ru^{3+} + 3OH^- \rightarrow Ru(OH)_3 \quad (3)$$

The excess of anions (OH^-) reacts with ruthenium hydroxide and converts it to ruthenium oxide, according to the folowing reaction:

$$Ru(OH)_3 + OH^- \rightarrow RuO_2 + 2H_2O \quad (4)$$

A prepared dark aqueous solution was sprayed onto ordinary glass substrates, pre-heated at 350 °C, for 5 min. The spray flow was of 2.6 ml/min. Dark amorphous ruthenium oxide layers were obtained, then were heat treated under sulfur atmosphere (~10^{-6} torr) at various sulfurization temperatures (400, 450, 500, and 550 °C) for 3 hours in RTP oven. The as-obtained ruthenium sulfide films were characterized using the X-ray diffractometer (D8 Advance Bruker) with Cu-Kα radiation operated at 40 KV and 40 mA (λ=1.5418 Å) in 2θ range 20°-70°, for analyzing the crystalline structure. Optical properties (transmittance and reflectance) were measured at normal incidence with a UV-VIS-NIR spectrophotometer Model Shimadzu 3100S for the wavelength range from 300 to 1,800 nm. Moreover, their electrical properties were determined using the four-point method. Finally, electronic scanning microscopy (SEM) equipped with energy dispersive spectroscopy (EDS) was used for studying the surface morphology and element compositions of the obtained ruthenium sulfide thin films.

RESULTS AND DISCUSSION

1. Structure and Texture

After preliminary experiences for adaptation of the deposition parameters, we succeeded to obtain the ruthenium disulfide layers. To identify the obtained phases, the as-prepared films were characterized by XRD. Kratzig et al. [19] noted that the obtained RuS_2 crystallizes in the cubic space group: Pa-$\bar{3}$ (laurite, JCPDS-Card Number 00-012-0737). Its lattice constant is a=5.6180 Å. After sulfurization under vacuum at different temperatures (400, 450, 500 and 550 °C) for 3 hours in an RTP oven, of the pre-sprayed amorphous ruthenium oxide layers, the obtained films were character-

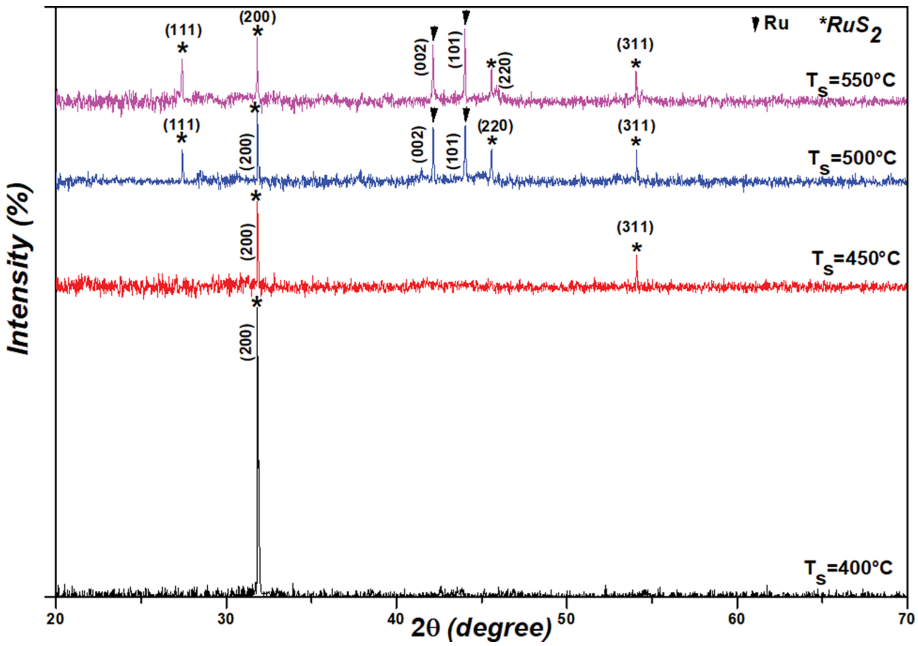

Fig. 1. XRD diagrams of RuS_2 thin films obtained by sulfurization, under vacuum at different sulfurization temperatures (400, 450, 500, and 550 °C) for 3 hours in RTP oven, of amorphous ruthenium oxide layers pre-deposited on glass substrates.

ized by XRD. The corresponding patterns are shown in Fig. 1. Therefore, we concluded that all the obtained samples at different sulfurization temperatures presented peaks of RuS_2 (laurite, JCPDS-Card Number 00-012-0737), but with different intensities and orientations. Then, at 400 °C an intensive peak was detected at 2θ= 31.82° with the orientation (200) corresponding to RuS_2 peak, which points at a higher degree of crystallinity. In this case, the existence of a single orientation of RuS_2 shows that the formed ruthenium disulfide is monocrystalline. At 450 °C, the samples show the diffraction lines of RuS_2 phase with the characteristic peak at $2\theta\cong$ 31.818°, having a lower intensity than that at 400 °C at the same 2θ value, which corresponds to the (200) orientation. A second peak at 2θ=54.060° according to the (311) orientation. At 500 °C, the samples show the diffraction lines of RuS_2 with the characteristic peaks at 2θ=27.421° (111), 2θ=31.817° (200), 2θ=54.060° (311), and a weaker one at 2θ=45.571° that corresponds to the (220) orientation. Furthermore, additional diffraction peaks of metallic ruthenium (JCPDS No: 00-006-0663) appeared, while the intensity of RuS_2 peaks drops off significantly. Indeed, obviously at substrate temperatures higher than 500 °C, the RuS_2 is no longer stable under these sulfurization conditions (vacuum ~10^{-6} torr, spray with a gas vector: Compressed air) and decomposes on the substrate to metallic ruthenium. Then, the EDX analysis of the samples obtained at these higher sulfurization temperatures reveals a considerable increase of the ratio: Ru/S. At the sulfurization temperature of 550 °C, the same peaks as those obtained at 500 °C are present but with small difference of intensity. The existence of several orientations of RuS_2, in the case of the samples obtained after sulfurization at the temperatures of 500 °C and 550 °C, shows a polycrystalline material. These results were deduced by other researchers [31].

To confirm the good crystallinity of the obtained layers, Table 1 presents the half maximum intensity (FWHM) of the line having the highest intensity, on the XRD diagrams, calculated for all the obtained RuS_2 films. The obtained results (Table 1) confirm the good crystallinity of the samples obtained after sulfurization at 400 °C. Indeed, the highest peak on the XRD diagram of the pre-cited films presents the lowest value of the half maximum intensity, which confirms that the crystallinity obtained at this temperature was the best. The decrease of the crystallinity when the sulfurization temperature increases confirms also the decomposition of RuS_2 on the substrates.

2. Morphological Characterization

To investigate the morphology of the obtained ruthenium disulfide thin films, scanning electron microscopy (SEM) was performed employing a Thermo Scientific Q250 SEM. This microscope is also

Table 1. Half maximum intensities (FWHM) of the lines having the highest intensity on the XRD diagrams of the RuS_2 films, obtained by sulfurization under vacuum at different temperatures (400, 450, 500 and 550 °C) for 3 hours in an RTP oven, of amorphous ruthenium oxide thin films, pre-sprayed on glass substrates

Sulfurization temperature (°C)	hkl	2θ (°)	FWHM (°)
400	200	31.8467	0.1624
450	200	31.7591	0.656
500	200	31.7175	0.8983
550	200	31.8403	0.5665

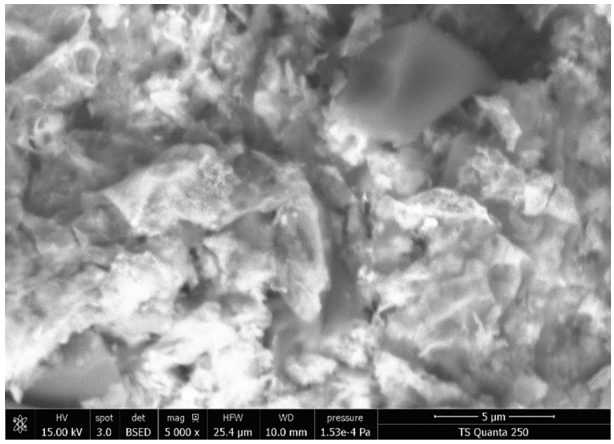

Fig. 2. SEM micrograph of RuS_2 thin films obtained by sulfurization, under vacuum at 400 °C for 3 hours in an RTP oven, of amorphous ruthenium oxide layers pre-deposited on glass substrates.

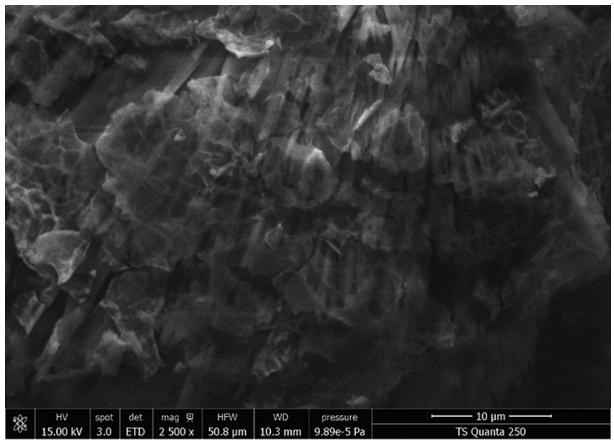

(a)

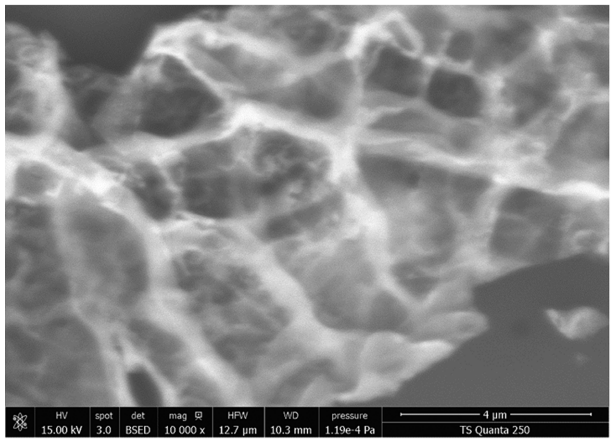

(b)

Fig. 3. SEM micrographs of RuS_2 thin films obtained by sulfurization, under vacuum at 450 °C for 3 hours in RTP oven, of amorphous ruthenium oxide layers pre-deposited on glass substrates by spray pyrolysis.

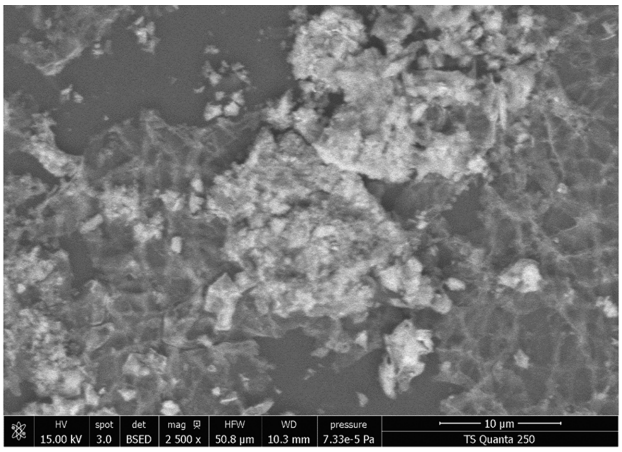

(a)

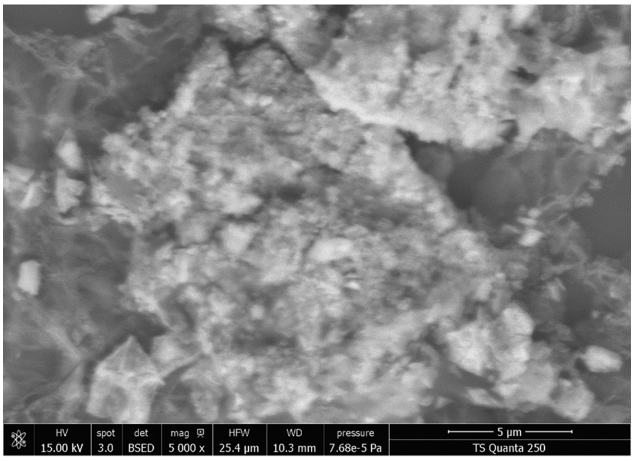

(b)

Fig. 4. SEM micrographs at different magnifications of RuS_2 thin films obtained by sulfurization, under vacuum at 500 °C for 3 hours in RTP oven, of amorphous ruthenium oxide layers pre-deposited on glass substrates by spray pyrolysis.

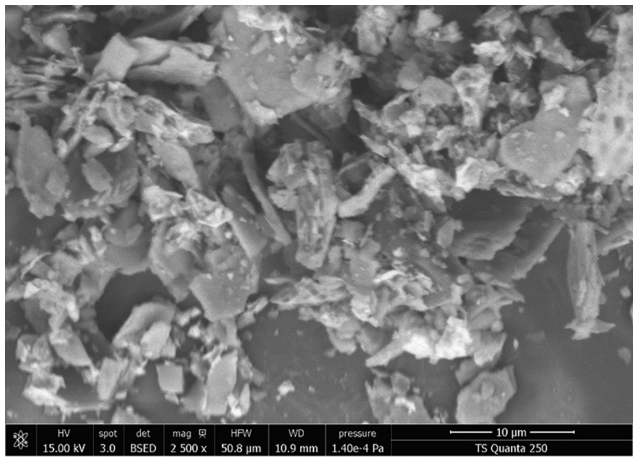

(a)

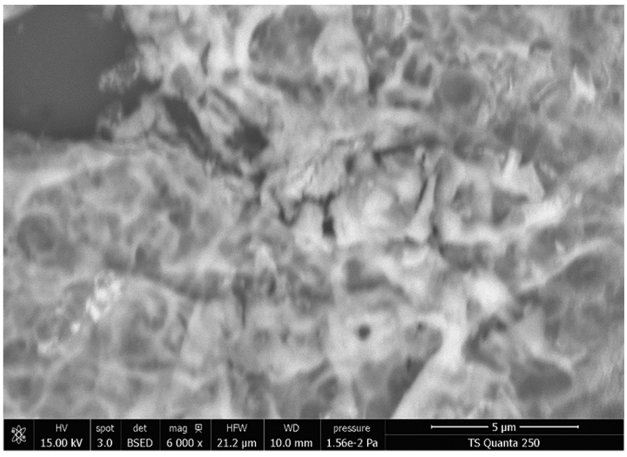

(b)

Fig. 5. SEM micrographs at different magnifications of RuS_2 thin films obtained by sulfurization, under vacuum at 550 °C for 3 hours in RTP oven, of amorphous ruthenium oxide layers pre-deposited on glass substrates.

equipped with a system for energy dispersive X-ray fluorescence analysis (EDX, Thermo Scientific), which is used to determine the composition of the samples. The obtained scanning electron micrographs of the as-deposited thin films are shown in the Figs. 2, 3, 4, and 5. SEM images for all the obtained layers showed a mix of morphologies (filament, particles, and clusters) with porous surfaces. At the sulfurization temperature of 400 °C (Fig. 2), the samples show clustered structure with a good adherence to the substrate. A strong porosity is observed, as well. However, the layers obtained at the sulfurization temperature of 450 °C (Fig. 3(a)), present a filament structure that can clearly be seen at high magnification (Fig. 3(b)). The samples sulfurized at 500 °C (Fig. 4(a)) show clusters interconnected and filaments. Fig. 4(b) shows that the layers consisted of particles also. At the sulfurization temperature of 550 °C (Fig. 5(a)), the samples show clusters interconnected with each other. But, at high magnification (Fig. 5(b)) it appears that the layer morphology consists of a mixture of clusters and filaments covering well the substrate. The porous surface promotes the permeability of solar rays, which increases the conductivity of the layers.

Table 2. EDS analysis of the RuS_2 films obtained after sulfurization under vacuum at different temperatures (400, 450, 500 and 550 °C) for 3 h in an RTP oven, of amorphous ruthenium oxide thin films

400 °C	Element	Net counts	Weight %	Atom %	(Ru/S)%
	Ru	23,905	52.91	20.30	0.508
	S	26,783	24.61	39.96	
450 °C	Element	Net counts	Weight %	Atom %	(Ru/S)%
	Ru	18,968	54.49	20.42	0.496
	S	25,489	29.75	41.15	
500 °C	Element	Net counts	Weight %	Atom %	(Ru/S)%
	Ru	19,324	50.02	20.32	0.495
	S	25,376	29.89	40.97	
550 °C	Element	Net counts	Weight %	Atom %	(Ru/S)%
	Ru	18,369	50.59	21.81	0.543
	S	25,231	29.53	40.13	

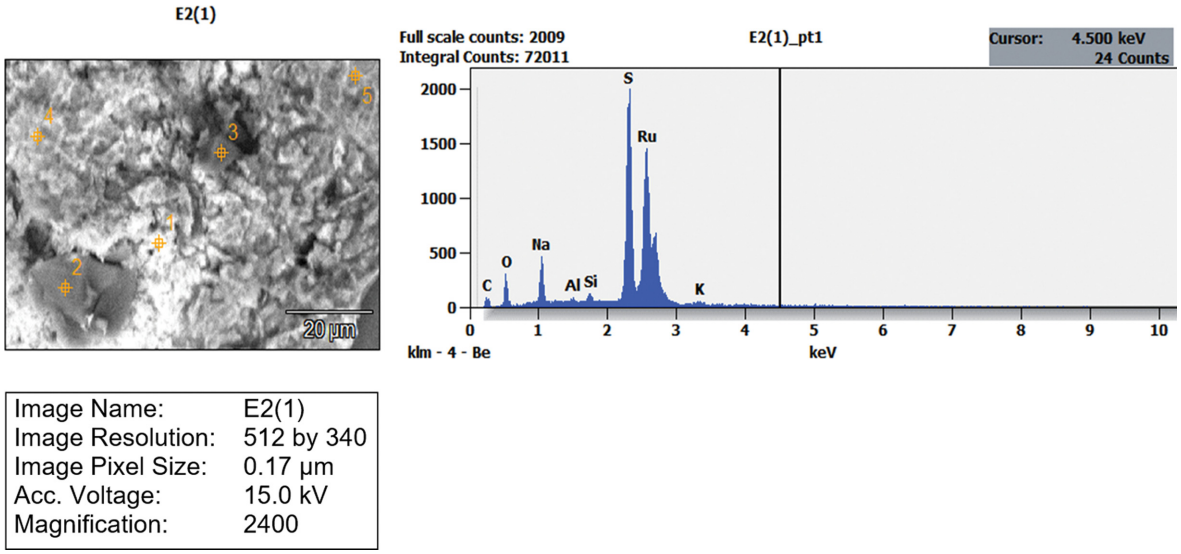

Fig. 6. EDX spectrograph of the ruthenium disulfide layers obtained after heat treatment at 400 °C under sulfur atmosphere (~10^{-4} Pa) for 3 h in RTP oven of the pre-sprayed amorphous ruthenium oxide thin films.

SEM images prove that the samples obtained at the sulfurization temperature of 400 °C present the best morphology, because of their surface porosity. These results confirm those obtained by X-ray diffraction. In Table 2, after consideration of a slight amount of Ru that could be contributing to the ruthenium oxide (it was not detected by XRD), the ratio Ru/S was determined by EDX (Fig. 6) and is approximately 1 : 2 (Ru : S), which confirms the stoichiometry of the RuS_2 phase. Indeed, the ratio Ru : S was (1 : 1.968) and (1 : 2.016), for the samples obtained, respectively, at the sulfurization temperatures 400 °C and 450 °C, where only the RuS_2 phase appeared. The strange morphology observed at the higher temperatures of 500 °C and 550 °C confirms the appearance of ruthenium that has become an abundant component after decomposition of RuS_2 at these temperatures as explained according to the EDX and XRD results.

3. Optical Measurements

We took transmission and reflectivity measurements for all the prepared samples of the as-prepared ruthenium disulfide thin films, obtained by sulfurization under vacuum (~10^{-4} Pa) at various temperatures (400, 450, 500 and 550 °C) for three hours in RTP oven, of the amorphous ruthenium oxide pre-deposited by spray pyrolysis. The spectrophotometer used was a Shimadzu 3100S. Then, we determined the absorption coefficient and the possible transitions (Eq. (5)). Fig. 7(a) and Fig. 7(b) show, respectively, the transmission and the reflectivity variations versus the wavelength (300 nm-1,800 nm). Therefore, lower transmission and reflectivity percentages are noted for all the prepared RuS_2 films, which proves their high absorbance. Those of the layers obtained at the sulfurization temperature of 400 °C were the lowest ones. However, the reflectivity of the layers obtained at the sulfurization temperature of 450 °C could be considered as the highest.

Using Eq. (5) to determine the absorption coefficient, all the layers seem to be highly absorbent. Indeed, a strong absorption is pointed out ($\alpha > 10^4$ cm^{-1}), so one must use Eq. (6) to determine the absorption of the RuS_2 layers obtained in the present work.

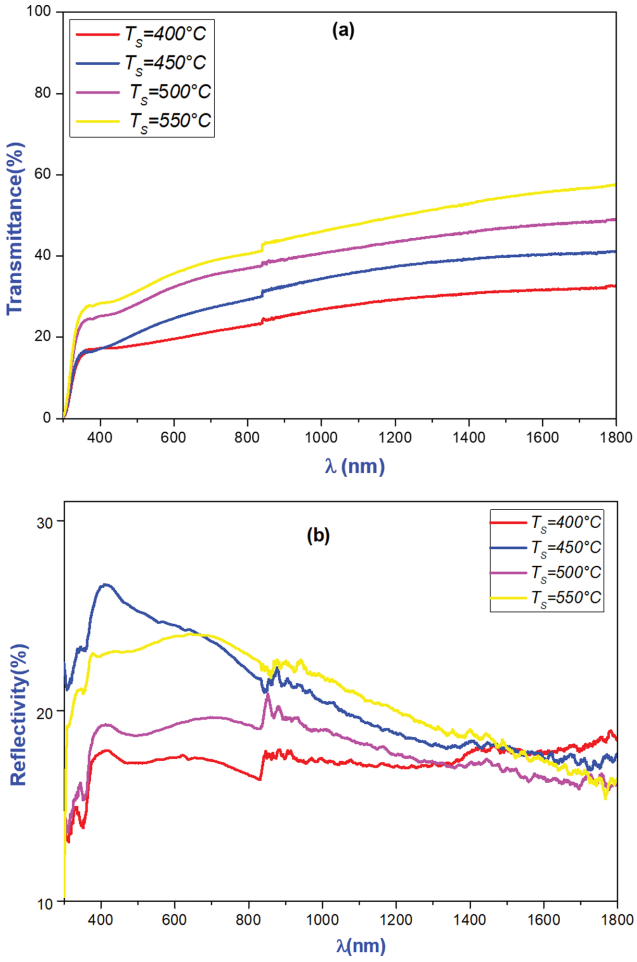

Fig. 7. Transmittance (a) and reflectivity (b) spectra of the ruthenium disulfide layers obtained after heat treatment at different temperatures (400 °C, 450 °C, 500 °C, 550 °C) under sulfur atmosphere (~10^{-4} Pa) for 3 h in RTP oven of the pre-sprayed amorphous ruthenium oxide thin films.

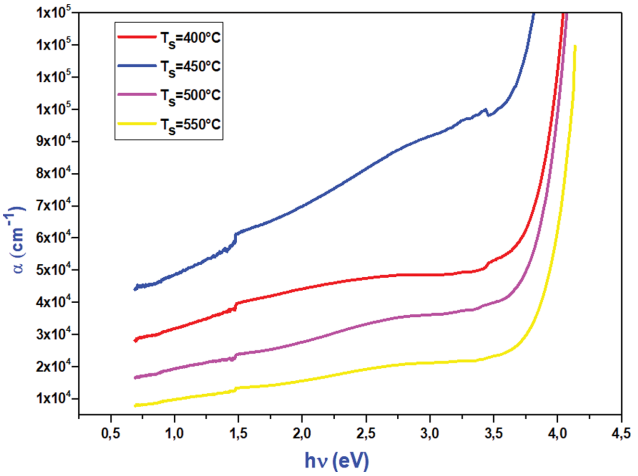

Fig. 8. Absorption coefficients of RuS_2 thin films obtained by sulfurization, at various annealing temperatures (400 °C, 450 °C, 500 °C, 550 °C) under vacuum (~10^{-4} Pa) for 3 hours in RTP oven, of pre-sprayed amorphous ruthenium oxide thin films.

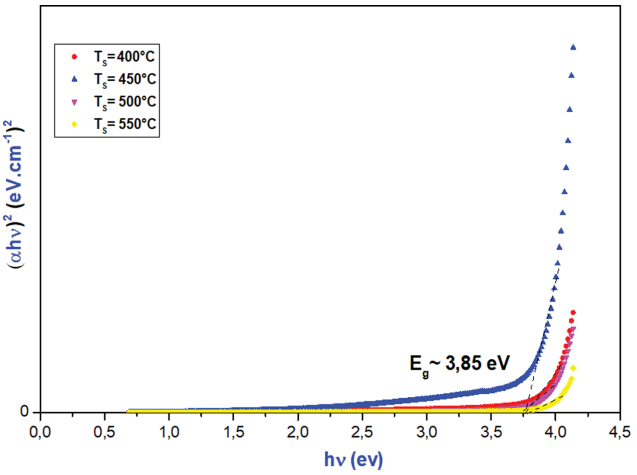

Fig. 9. Plots of $(\alpha \cdot h \cdot \nu)^2$ versus the photon energy $h\nu$, of the sulfurized ruthenium oxide films under vacuum at different temperatures (400, 450, 500, and 550 °C) for 3 hours in an RTP oven.

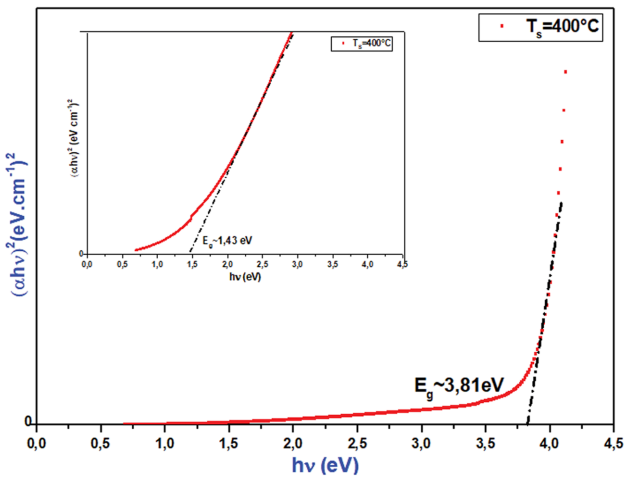

(a)

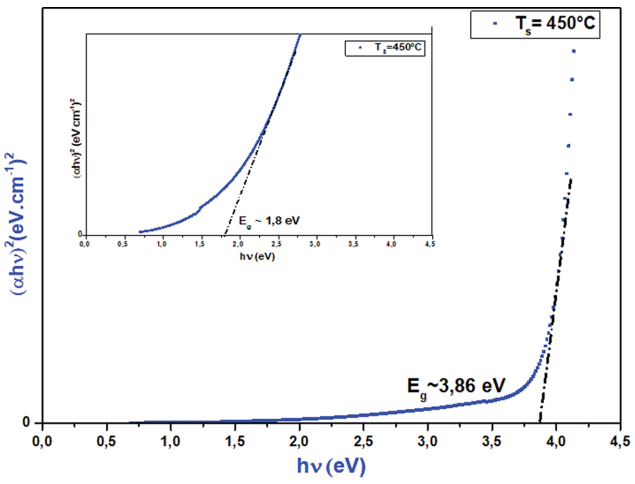

(b)

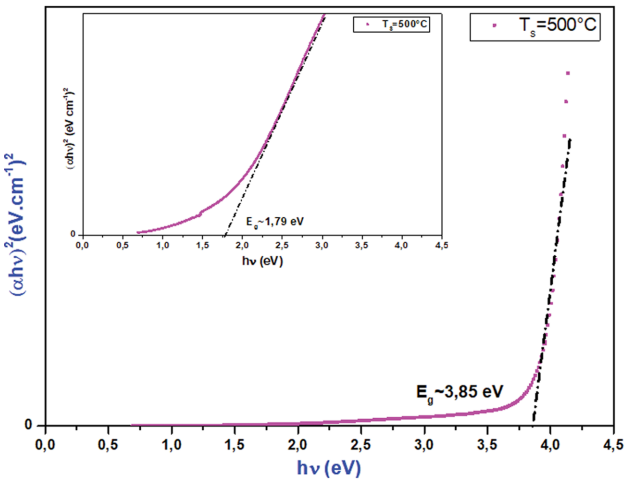

(c)

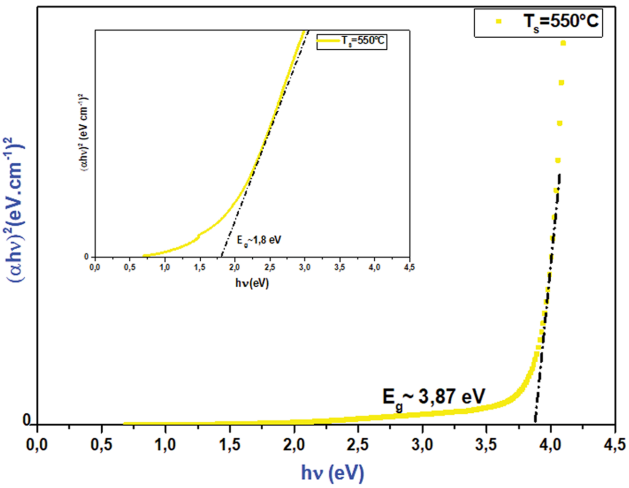

(d)

Fig. 10. Plot of $(\alpha \cdot h \cdot \nu)^2$ versus the photon energy $h\nu$, of the sulfurized ruthenium oxide films under vacuum at: (a) 400 °C, (b) 450 °C, (c) 500 °C, and (d) 550 °C, for 3 hours in an RTP oven.

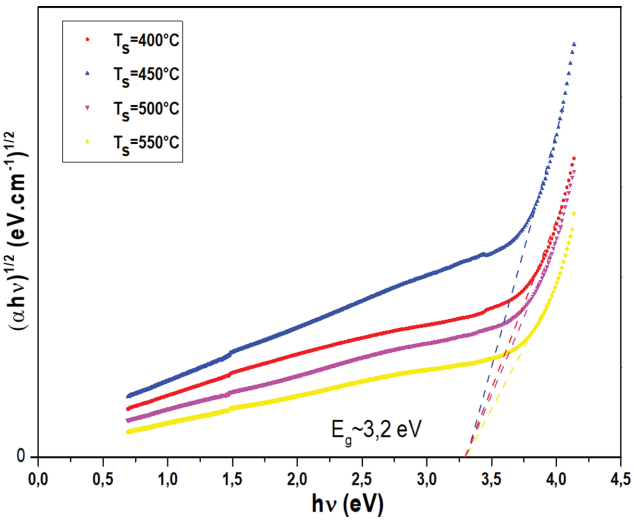

Fig. 11. Plots of $(\alpha \cdot h \cdot \nu)^2$ versus the photon energy $h\nu$, of the sulfurized ruthenium oxide films under vacuum at different temperatures (400, 450, 500, and 550 °C) for 3 hours in an RTP oven.

$$T = (1-R)^2 \exp(-\alpha d) \rightarrow \alpha = \frac{1}{d} \ln \frac{(1-R)^2}{T} \quad (5)$$

$$T = \frac{(1-R)^2 \exp(-\alpha d)}{1-R^2 \exp(-2\alpha d)} \rightarrow \alpha = \frac{1}{d} \ln \left[\frac{(1-R)^2}{T} + \left(\frac{(1-R)}{4T^2} + R^2 \right)^{0.5} \right] \quad (6)$$

where, T is the transmission coefficient, R represents the reflectivity, and d is the sample thickness, which was measured, using a profilometer, of about 350 nm. The absorption coefficient variations of the of the RuS_2 thin films, obtained at the different sulfurization temperatures (400, 450, 500 and 550 °C), versus the incident photon energy ($h\nu$) are shown in Fig. 8. Therefore, all the obtained layers show a high absorption coefficient ($\alpha > 10^4$ cm^{-1}, λ<1,300 nm). Figs. 9, 10, and 11 show the plots of $(\alpha \cdot h \cdot \nu)^{n/2}$ versus the photon energy, $h\nu$, with n=1 and n=4. Therefore, variation of $(\alpha h\nu)^2$ versus $h\nu$ gives two straight lines for the samples sulfurized at the different temperatures (Fig. 9), suggesting that each layer presents two direct transitions. Fig. 10(a) shows that RuS_2 thin films, obtained at 400 °C, present a first direct transition corresponding to a photon energy of about 1.43 eV and a second one corresponding to an energy of about 3.31 eV. Whereas those obtained at 450 °C (Fig. 10(b)), present a first direct transition corresponding to the energy of about 1.80 eV and the second corresponds to the energy of about 3.86 eV. At the sulfurization temperatures of 500 °C and 550 °C, the obtained samples present two direct transitions at each temperature, also, (Fig. 10(c), Fig. 10(d)). Indeed, at 500 °C, the corresponding energies are 1.79 eV and 3.85 eV, and at 550 °C the corresponding energies are: 1.8 eV and 3.87 eV. Whereas, at the different temperatures, the obtained material presents an indirect transition corresponding to a photon energy of about 3.2 eV (Fig. 11). Hence, one can see that the obtained RuS_2 at the different sulfurization temperatures 400, 450, 500 and 550 °C, presents direct band gap, corresponding to the photon energies of, respectively, 1.43, 1.80, 1.79, and 1.80 eV. Similar results were observed by several researchers [1,8,15,32,33]. Thus, the RuS_2 thin films, obtained at the sulfurization temperature of 400 °C present a band gap energy of 1.43 eV, a desired value for photovoltaic applications such as solar cells. Moreover, the band gap energies, of the samples obtained at the other sulfurization temperatures (450 °C, 500 °C, and 550 °C) may be considered as desired values for several applications.

4. Electrical Transport Properties

Using the Hall effect measurements. After applying a magnetic field, B=0.554T, and an initial current of 1 μA, the resistivity and the conductivity values of the as prepared RuS_2 thin films were obtained and given in Table 3. The obtained RuS_2 thin films show n-type semi-conductor behavior and their mobility ranges from 0.675 to 4.870 cm^{2}V^{-1} S^{-1}. Their electrical resistivity decreases with increase in the sulfurization temperature from 400 °C to 500 °C and ranges from 48.591 Ω cm (at 400 °C) to 33.302 Ω cm (at 500 °C), which proves the semiconductor behavior of the RuS_2 thin films in this region of temperature. But, with increase in the sulfurization temperature from 500 °C to 550 °C, the electrical resistivity of the obtained films increases to reach 43.375 Ω cm (at 550 °C), which shows metallic behavior [16,34,35]. Consequently, a semiconductor-to-metal transition [36]. The conductivity increases from 2.058 10^{-2} S·m^{-1} (at 400 °C) to 3.0028 10^{-2} S·m^{-1} (at 500 °C. Then, decreases to reach 2.305 10^{-2} S·m^{-1} (at 550 °C). The semiconductor-to-metal transition was observed with a decrease in the sheet concentration by about 100 times its magnitude. Therefore, the bulk concentration is about 1.118 10^{18} cm^{-3}, at 400 °C, about 3.848 10^{16} cm^{-3}, at 500 °C, and about 6.887 10^{16} cm^{-3} at 550 °C. This shows also a decrease by about 100 times its magnitude during this semiconductor-to-metal transition. These obtained electrical results confirm that 400 °C is the best sulfurization temperature during the present work and confirm the results obtained by X-ray diffraction, SEM and optical measurements.

CONCLUSION

RuS_2 has several properties making it a precious material in the photovoltaic field, and to be shown as the most active catalyst for hydrodesulfurization processes. Therefore, we are interested in this research work in the growth of RuS_2 thin films using a very sim-

Table 3. Resistivity and conductivity values of the RuS_2 films obtained after sulfurization under vacuum at different temperatures (400, 450 and 500 °C) for 3 h in an RTP oven, of amorphous ruthenium oxide thin films pre-deposited on glass substrates

Sulfurization temperature (°C)	Resistivity (Ω cm)	Conductivity (S·m^{-1})	Mobility (cm^{2}V^{-1}S^{-1})	Sheet concentration (cm^{-2})	Bulk concentration (cm^{-3})
400	48.591	2.058 10^{-2}	0.67542	−3.5020E+13	−1.1188E+18
450	33.302	3.0028 10^{-2}	4.870	−6.3892 10^{11}	−3.848 10^{16}
500	43.375	2.305 10^{-2}	2.089	−2.135 10^{12}	−6.887 10^{16}

ple and non-cost technique: spray pyrolysis. X-ray diffraction studies showed that the growth of monocrystalline and polycrystalline RuS_2 thin films depends on the heat treatment temperature. Moreover, these characterizations revealed preferred growth of RuS_2 with (200) orientation at a sulfurization temperature of 400 °C. It was shown also that the crystallinity of the layers obtained at this temperature was the best. Scanning electron microscopy showed for all the obtained layers a mix of morphologies (filament, particles, and clusters) with porous surfaces. The results of optical absorption measurements indicated a high absorbance ($\alpha > 10^4$ cm^{-1}) and a direct band gap for all the obtained layers. According to the variation of the sulfurization temperature, the deduced band gap energies were of about 1.43 eV at a sulfurization temperature of 400 °C, which can be evaluated as an interesting result. The same is for the layers obtained at the other temperatures and presenting a direct band gap about 1.80 eV. The most interesting result during this experimental work is the use of a simple and efficient technique for obtaining RuS_2 thin films at lower temperatures compared to the work done before, and having desired properties for several applications, which make this technique distinguished. The opto-electrical properties of the as-obtained RuS_2 thin films make them among the best candidates for several applications, such as low cost material for low cost solar cells, and alkaline hydrogen evolution (HER) electrocatalysts.

ACKNOWLEDGEMENTS

Our thanks and our appreciation to the staff of the "L.P.V, Centre de Recherches et des Technologies de l'Énergie, Technopole de Borj-Cédria" and specially the Director, Pr. Mongi Bouaicha, for the support. Our deep gratitude and regard to Mr. Taoufik Bouaanane, for his precious electrical measurements. We would like to take this opportunity to express our gratitude and regard to Pr. Kamel Khirouni, Pr. Noureddine Bouguila, and Dr. Belgacem Tiss, "Laboratory of Physics of Materials and Nanomaterials Applied at Environment-Faculty of Sciences in Gabes, for their support.

REFERENCES

1. M. Ashokkumar, A. Kudo, N. Saito and T. Sakata, *Chem. Phys. Lett.*, **229**(4-5), 383 (1994).
2. K. Krishnamoorthy, P. Pazhamalai and S. J. Kim, *Electrochim. Acta*, **227**, 85 (2017).
3. S. Licht, S. Ghosh, H. Tributsch and S. Fiechter, *Sol. Energy Mater. Sol. Cells*, **70**(4), 471 (2002).
4. M. E. Grillo, V. Smelyanski, P. Sautet and J. Hafner, *Surf. Sci.*, **439**(1-3), 163 (1999).
5. J. A. De Los Reyes, *Appl. Catal. A-Gen.*, **322**, 106 (2007).
6. S. Baurier-Aymat, A. Jiménez-Franco, J. Roqué-Rosell, J. M. González-Jiménez, F. Gervilla, J. A. Proenza and F. Nieto, *Minerals*, **9**(5), 288 (2019).
7. M. Y. Tsay, S. H. Chen, C. S. Chen and Y. S. Huang, *J. Cryst. Growth*, **144**(1-2), 91 (1994).
8. H. Ezzaouia, R. Heindl, R. Parsons and H. Tributsch, *J. Electroanal. Chem.*, **145**(2), 279 (1983).
9. S. Brunken, A. Kratzig, P. Bogdanoff, S. Fiechter and K. Ellmer, *Thin Solid Films*, **527**, 16 (2013).
10. Z. Y. Feng, Y. Yang and J. M. Zhang, *J. Phys. Chem. Solids*, **129**, 227 (2019).
11. D. Eliche-Quesada, E. Rodríguez-Castellón and A. Jiménez-López, *Micropor. Mesopor. Mater.*, **99**, 268 (2007).
12. M. Aouine, C. Geantet and T. Epicier, *Catal. Today*, **66**(1), 91 (2001).
13. S. E. Skrabalak and K. S. Suslick, *J. Am. Chem. Soc.*, **127**(28), 9990 (2005).
14. T. Cai, Z. Song, J. A. Rodriguez and J. Hrbek, *J. Am. Chem. Soc.*, **126**(29), 8886 (2004).
15. H. Ezzaouia, J. W. Foise and O. Gorochov, *Mater. Res. Bull.*, **20**(11), 1353 (1985).
16. N. Tomar, A. Agrawal, V. S. Dhaka and P. K. Surolia, *Sol. Energy*, **207**, 59 (2020).
17. N. A. W. Holzwarth, S. Harris and K. S. Liang, *Phys. Rev. B*, **32**(6), 3745 (1985).
18. H. Colell and N. Alonso-Vante, *Electrochim. Acta*, **38**(14), 1929 (1993).
19. A. Kratzig, C. Zachäus, S. Brunken, D. Thomas, P. Bogdanoff, K. Ellmer and S. Fiechter, *Phys. Status Solidi (a)*, **211**(9), 2020 (2014).
20. W. Luo, Y. Wang and C. Cheng, *Mater. Today Phys.*, 100274 (2020).
21. J. D. Passaretti, R. C. Collins, A. Wold, R. R. Chianelli and T. A. Pecorara, *Mater. Res. Bull.*, **14**(9), 1167 (1979).
22. N. Le Nagard, A. Bouanani, H. Ezzaouia and O. Gorochov, *J. Cryst. Growth*, **104**(2), 365 (1990).
23. Y. S. Huang and Y. F. Chen, *Phys. Rev. B*, **38**(12), 7997 (1988).
24. B. Ouertani, J. Ouerfelli, M. Saadoun, B. Bessaïs, H. Ezzaouia and J. C. Bernède, *Sol. Energy Mater. Sol. Cells*, **87**, 501 (2005).
25. B. Ouertani, J. Ouerfelli, M. Saadoun, B. Bessaïs, H. Ezzaouia and J. C. Bernède, *Mater. Lett.*, **59**, 734 (2005).
26. B. Ouertani, H. Ezzaouia and B. Theys, *Colloids Surf. A: Physicochem. Eng. Asp.*, **525**, 13 (2017).
27. B. Ouertani, G. Bidouk, R. Ouertani, B. Theys and H. Ezzaouia, *Mater. Chem. Phys.*, **242**, 122272 (2020).
28. E. Djatoubai and J. Su, *Chem. Phys. Lett.*, **770**, 138406 (2021).
29. B. Ouertani, H. Boughzala, B. Theys and H. Ezzaouia, *J. Alloys Compd.*, **871**, 159490 (2021).
30. V. D. Patake and C. D. Lokhande, *Appl. Surf. Sci.*, **254**, 2820 (2008).
31. P. Bogdanoff, C. Zachäus, S. Brunken, A. Kratzig, K. Ellmer and S. Fiechter, *Phys. Chem. Chem. Phys.*, **15**(5), 1452 (2013).
32. S. S. Lin, Y. S. Huang, C. R. Huang and M. C. Lee, *Solid State Commun.*, **69**(6), 589 (1989).
33. R. Bichsel, F. Levy and H. Berger, *J. Phys. C Solid State Phys.*, **17**(1), L19 (1984).
34. S. Mumtaz, M. Farooq Warsi, M. Naeem Ashiq, N. Karamat and I. Shakir, *Optoelectron. Adv. Mater.-Rapid Commun.*, **9**, 404 (2015).
35. S. Mumtaz, M. Ashiq, B. Ahmad, M. Faheem Ashiq, R. Sehrish Gohar, N. Nazar, S. H. Abdel-hafez, W. A. El-Sayed and I. Ahmad, *Appl. Phys. A*, **127**(12), 1 (2021).
36. D. N. Bose, B. Seishu, G. Parthasarathy and E. S. R. Gopal, *Proc. R. Soc. A: Mathematical, Phys. Eng. Sci.*, **405**, 345 (1829).